JACS
JOURNAL OF THE AMERICAN CHEMICAL SOCIETY
Article
pubs.acs.org/JACS

Reversible Aromaticity Transfer in a Bora-Cycle: Boron–Ligand Cooperation

Urs Gellrich,[†] Yael Diskin-Posner,[‡] Linda J. W. Shimon,[‡] and David Milstein*[,†]

[†]Department of Organic Chemistry and [‡]Department of Chemical Research Support, Weizmann Institute of Science, Rehovot 76100, Israel

Supporting Information

ABSTRACT: Aromaticity is a central concept in chemistry. Reaction pathways involving reversible ligand dearomatization sequences emerged as a powerful tool for bond activation by metal complexes. Exploring this concept with a metal-free system, we have synthesized a pyridine-coordinated amino-borane which undergoes a temperature-induced formal dearomatization of the pyridine ring. NMR studies and DFT calculations revealed that this formal dearomatization sequence led to an aromaticity switch and the formation of a six-π-electron boron-containing heteroaromatic system. Disrupting this aromatic system by coordination of an amine or a carboxylic acid to the boron center enabled N–H activation and O–H cleavage, leading to an unprecedented reversal aromaticity switch.

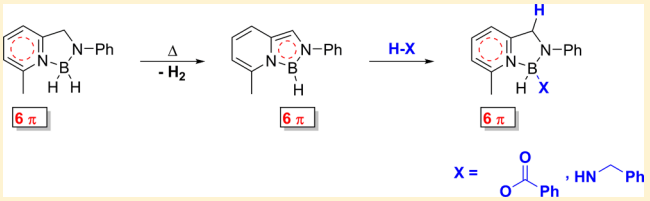

INTRODUCTION

Metal–ligand cooperation has emerged as a powerful tool for bond activation.[1,2] Examples include metal–amine/amide complexes able to activate H_2 and N–H sigma bonds as well as metal–alkoxide/alcohol complexes which were used to activate the O–H σ-bond of alcohols.[3−5] Many of the bond activations enabled by metal–ligand cooperation are assumed to be of vital importance for catalysis.[1] In 2005, our group discovered that ruthenium pincer complexes with a pyridine ring in the ligand backbone can undergo a reversible dearomatization sequence with liberation of hydrogen (Scheme 1).[6]

Scheme 1. Reversible Aromatization of a Pyridine-Based Ruthenium Pincer Complex

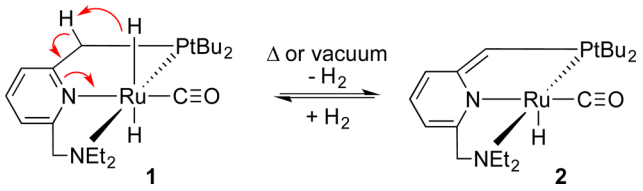

Complex **2** also activates the O–H σ-bond of water via rearomatization, which is assumed to be essential for the light-induced water splitting reported with this complex.[7] Notably, **2** catalyzes amide formation from alcohols and amines with liberation of H_2.[8] Mechanistic studies revealed that the catalytic cycle includes metal–ligand cooperation via several dearomatization and rearomatization sequences involving O–H σ-bond activation.[9] The concept of reversible dearomatization was expanded to various ligands and transition metals capable of C–H,[10] N–H,[11] and B–H[12] σ-bond activation via this novel type of metal–ligand cooperation. A comprehensive overview, also focusing on the application of these systems in homogeneous catalysis, was reported recently.[13] In an interesting theoretical study, Wang et al. examined if the concept of bond activation via dearomatization/rearomatization can be transferred to metal free systems, specifically methylpyridine-coordinated boranes (Scheme 2).[14] They concluded that for the simple case of a methylpyridine·BH_3 complex the dearomatized form is too unstable most likely because of the formation of a three-coordinated boron species. We hypothesized that attaching a covalently bound nitrogen atom to the boron will stabilize the dearomatized form by electron donation from the lone pair of the nitrogen into the empty p-orbital of the boron.[15]

Scheme 2. Metal-Free System Theoretically Examined before[14] for Its Potential To Undergo Dearomatization with H_2 Liberation and the Potential Stabilization of the Dearomatized Form by Electron Donation from a Nitrogen Lone Pair to the Empty p-Orbital at the Boron Center Proposed Here

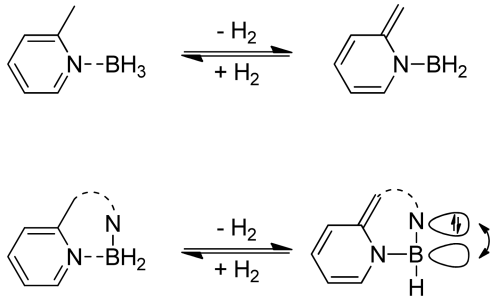

Received: July 22, 2016
Published: September 15, 2016

DOI: 10.1021/jacs.6b07454
J. Am. Chem. Soc. 2016, 138, 13307−13313

RESULTS AND DISCUSSION

To test this hypothesis, we synthesized aminoborane **6** (Scheme 3). After a reductive amination of 6-methylpyridine-2-carboxaldehyde **3** with aniline, the reaction of **4** with the *in situ* generated BH_2Br yielded salt **5**, which was directly deprotonated. Desired product **6** was purified by crystallization from CH_2Cl_2/pentane.

Scheme 3. Synthesis of the Aminoborane 6

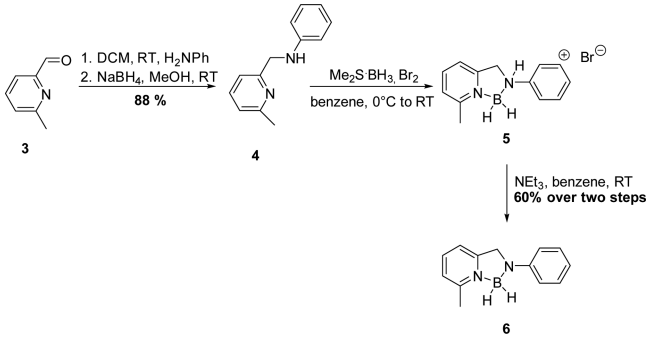

Compound **6** was characterized by ^{1}H, ^{11}B, ^{13}C, and HH–COSY NMR as well as IR spectroscopy. The structural assignment was furthermore supported by X-ray analysis (Figure 1).

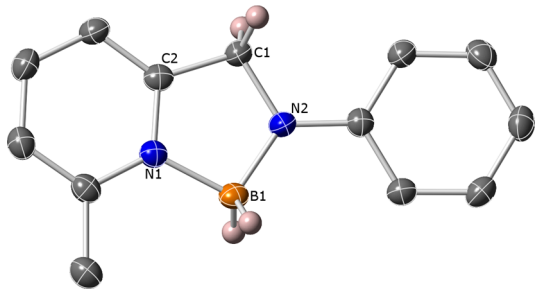

Figure 1. ORTEP representation of **6** (50% probability ellipsoids, all hydrogens but the ones on C1 and B1 are excluded for clarity). Selected bond lengths (Å) and angles (deg): N1–B1: 1.589(2), N2–B1: 1.534(3), N1–C2: 1.346(2), N2–C1: 1.456(2), C2–C1: 1.490(3), N1–B1–N2: 97.82(14), B1–N2–C1: 113.75(14), B1–N1–C2: 112.35(15).

^{11}B NMR of **6** shows a broad triplet at −2.6 ppm which becomes sharp at 333 K revealing a $^{1}J_{BH}$ coupling constant of 101.6 Hz. The chemical shift indicates a tetra-coordinated boron. Interestingly, when **6** was heated to 333 K for 16 h in C_6D_6, a new doublet at 19.70 ppm with a $^{1}J_{BH}$ coupling constant of 155.1 Hz was observed (Figure 2).

The presence of a $^{1}J_{BH}$ coupling shows that a BH bond is still intact, and the shift to lower field suggests a three-coordinated boron center. The ^{1}H NMR spectra of this new species not only showed chemical shifts and a splitting pattern strongly reminiscent of that of dearomatized ruthenium complex **2** but also revealed that the exocyclic methyl group is still present. When the reaction was performed in a closed system, hydrogen gas was detected by GC analysis of the headspace. We therefore assigned the new species to dearomatized aminoborane **7** (Scheme 4). While dearomatization sequences via intramolecular hydride shifts have been described, this is to the best of our knowledge the first example of a dehydrogenative dearomatization of a pyridine ring coordinated to a boron center.[16] This assignment is

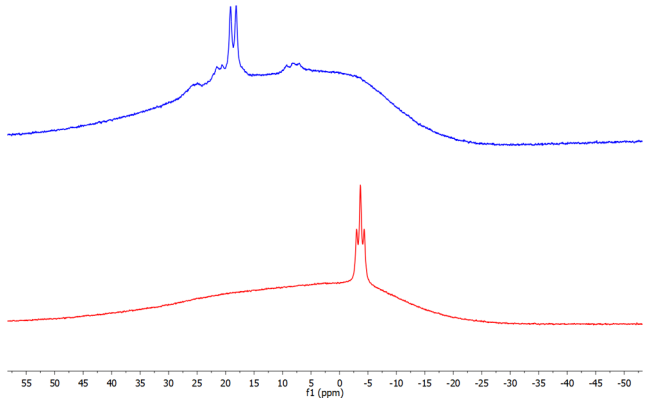

Figure 2. ^{11}B NMR spectrum of **6** (0.2 M in benzene-d_6) (bottom) at 333 K and the spectrum obtained after heating the sample for 16 h to 333 K (top).

Scheme 4. Observed Dehydrogenative Formal Dearomatization of 6

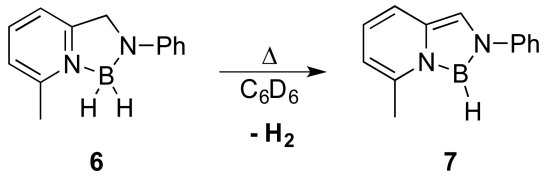

furthermore supported by a comparison of the experimentally found ^{11}B NMR shifts with those calculated at the M06-2X/def2-TZVPP level of theory (Table 1).

Table 1. Comparison of the Calculated ^{11}B NMR Shifts for 6 and 7 with the Experimentally Observed Chemical Shifts

	exp.	DFT[a]
6	−2.6	−4.1
7	19.7	21.0

[a]Referenced to $Me_3N{\cdot}BH_3$.

The BH stretching of **7** is blue-shifted compared to the BH stretching vibrations of **6**, indicating the formation of a sp^2-hybridized boron center. Furthermore, the experimental vibrations are found to be in good agreement with the calculated ones (Table 2).

Table 2. Comparison of the Calculated and the Experimentally Observed BH Stretching Vibrations of 6 and 7

	exp.	DFT[a]
6	2290	2338/2332 (2461/2455)
7	2607	2611 (2749)

[a]Calculated vibrations are scaled to account for anharmonicity; unscaled vibrations are given in parentheses.[17]

The mechanism of the temperature-induced formation of **7** remains unclear. DFT calculations suggest that a direct intramolecular H_2 elimination is unlikely.[18] An intramolecular mechanism akin to those operating in some frustrated Lewis acid base pairs is not supported by kinetic experiments.[19] The formation of **7** by heating a solution of **6** was however accompanied by the formation of unidentified impurities. Compound **7** was obtained in a cleaner form when a suspension

DOI: 10.1021/jacs.6b07454
J. Am. Chem. Soc. 2016, 138, 13307–13313

of **5** in toluene was stirred for 48 h at RT and then deprotonated with NEt_3. Samples of **7** obtained in this way were used for assignment of the ring protons and compared to the ^{1}H NMR spectrum of **6** (Figure 3).

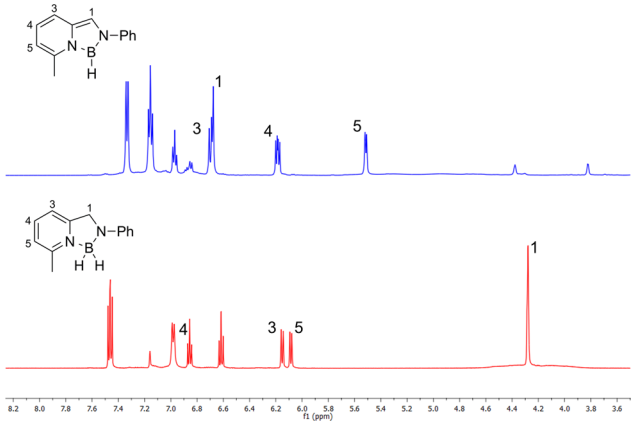

Figure 3. ^{1}H NMR spectra of **6** (bottom) and **7** (top) (0.2 M in benzene-d_6). The assignments of H3 and H5 can be interchanged.

The high-field shifts of the protons at C5 and C4 agree with the anticipated dearomatization of the pyridine ring. The C1 signal of **7** can now be found at 6.68 ppm, which is a rather unusual shift for a Csp_2–H signal. Indeed, when assuming that the boron center in **7** is sp^2-hybridized, the five-membered ring can be formally described as a six-π-electron Hückel aromatic system. Since proton shifts are not a sensitive indication of aromaticity, we decided to investigate the aromaticity of **6** and **7** by means of NICS (nucleus-independent chemical shifts) calculations.[20] Therefore, ghost atoms were placed in the center of both rings in **6** and **7**, and their isotropic shielding was computed (Table 3).

Table 3. Calculated NICS Values for the Six- and Five-Membered Rings in 6 and 7 (M06-2X/def2-TZVPP)

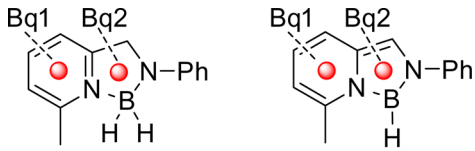

6 **7**

	6	7
Bq1	−6.0	0.1
Bq2	0.7	−10.9

As expected, the NICS calculations predict an aromatic character for the pyridine ring in **6** whereas the boron-containing five-membered ring is nonaromatic. In line with the assumption of a dearomatization, the former pyridine ring becomes non-aromatic in **7**. In contrast, remarkably, the boron-containing five-membered ring in **7** is clearly aromatic according to the NICS calculations. Boron-containing aromatic systems have recently attracted attention because of their interesting optoeletronic properties.[21] Significantly, whereas in the case of formally aromatic fused borepin rings, NICS calculations and experimental studies[21,22] reveal very weak or no local aromaticity character in the boron-containing ring: In the case of **7**, the NICS calculations show real local aromaticity akin to six-membered azaborines.[23]

According to the NICS calculations the former pyridine ring loses its aromaticity. This is an interesting finding since **7** could formally also be described as a 10-π-aromatic fused ring system. The dearomatization of the pyridine ring is indeed also reflected by the change in the carbon–carbon bond lengths: While they are almost identical in **6**, alternating bond lengths are present in the former pyridine ring in **7** (Table 4).

Table 4. Comparison of Calculated and Experimental Bond Lengths in the Pyridine Ring of 6 and 7

	6		7
	X-ray	DFT	DFT
C2–C3	1.384(3)	1.382	1.429
C3–C4	1.380(3)	1.384	1.348
C4–C5	1.385(3)	1.387	1.439
C5–C6	1.382(3)	1.386	1.349

The bond lengths for **7** are predicted by computation. A comparison of the experimentally determined and the calculated bond lengths of **6** show an excellent agreement. The level of theory seems therefore accurate enough to allow for the conclusion that bond length alternation in the pyridine ring occurs upon formation of **7**. In order to estimate the aromatic stabilization energy of the five-membered boron-containing ring in **7**, we applied the isomerization method, that is, calculating the energy of a hypothetical methyl and methylene derivative of **7** (Scheme 5).[24]

Scheme 5. Calculated ISE of 7 (M06-2X/def2-TZVPP)

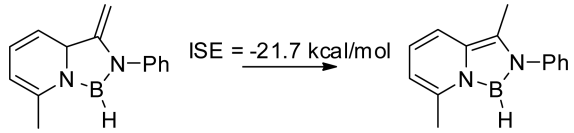

Although due to ring strain effects the absolute value might not allow for an accurate estimation of the aromatic stabilization energy of **7**, the significant isomerization stabilization energy (ISE) gives further evidence that **7** is indeed aromatic. The reaction is therefore better described as an "aromaticity shift" than as a dearomatization (Scheme 6). While ruthenium complex **2**

Scheme 6. Observed Aromaticity Switch upon Dehydrogenative Dearomatizaton of 6

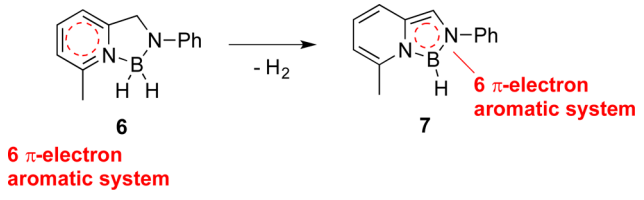

regenerates **1** via rearomatization under 1 bar H_2, **7** does not undergo any reaction under these conditions.[25] Assuming that coordination of an electron donor to the boron center in **7** will disturb its aromatic character, enabling the intended reverse of the aromaticity switch, we added 1.1 equiv of benzylamine to **7** and followed the reaction by ^{1}H NMR spectroscopy.

At 273 K, a new doublet appeared at 4.11 ppm (Figure 4). A COSY experiment revealed a cross peak to a broad signal at 3.47 ppm with a 1:2 integration ratio to the doublet at 4.11 ppm, which

DOI: 10.1021/jacs.6b07454
J. Am. Chem. Soc. 2016, 138, 13307–13313

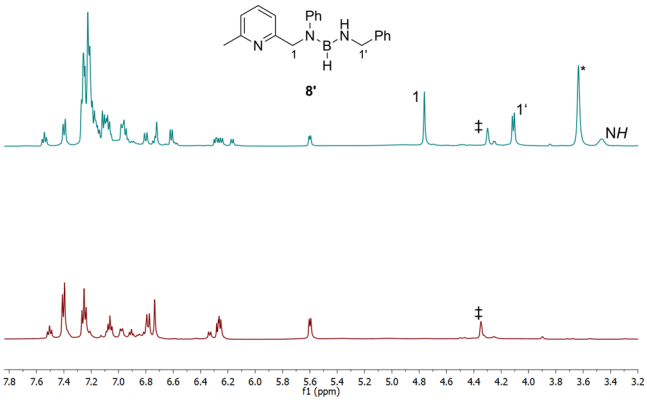

Figure 4. ^{1}H NMR spectra (toluene-d_8) of **7** (red) and 120 min after the addition of 1.1 equiv of benzylamine (green) at 273 K. Signals of **8′** are assigned. Peaks of **6** and benzylamine are marked with ‡ and *, respectively.

is therefore assigned to the CH_2 group of the former benzylamine. The broad signal at 3.47 ppm corresponds to a NH signal. The concomitant appearance of a sharp singlet at 4.76 ppm with a 2:2:1 integration ratio to the aforementioned signals indicates proton transfer from the NH_2 group of benzylamine to the Csp^2 group of the five-membered ring in **7**.

The new species is therefore assigned to be the benzylamine addition product **8** (Scheme 7). ^{11}B NMR of **8′** shows a broad signal at 30.0 ppm at 273 K (Figure 5). When the reaction mixture was heated to 333 K, this signal becomes a sharp doublet with a $^{1}J_{BH}$ coupling constant of 114.2 Hz. This shows that the BH bond is still intact. We assume that the temperature dependence of the line shape is caused by a hindered rotation of the pyridine ring coordinated to the boron. The chemical shift of 30.0 ppm is furthermore indicative for a three-coordinated boron center as indicated in Scheme 7 and Figure 4. This conclusion based on the ^{11}B NMR shift is in agreement with the relative energies of **8** and the open chain isomer **8′** calculated by DFT (see Figure 5).

Attempts to isolate **8′** in analytical pure form failed. However, further support for the assignment of the new species to **8′** comes from a comparison of the experimental and calculated ^{11}B NMR shifts and the BH and NH stretching vibrations (Table 5). While the ^{11}B NMR signal is shifted to lower field upon addition of benzylamine to **7**, the BH stretching vibration is red-shifted.[26]

Scheme 7. Reaction of 7 with Benzylamine

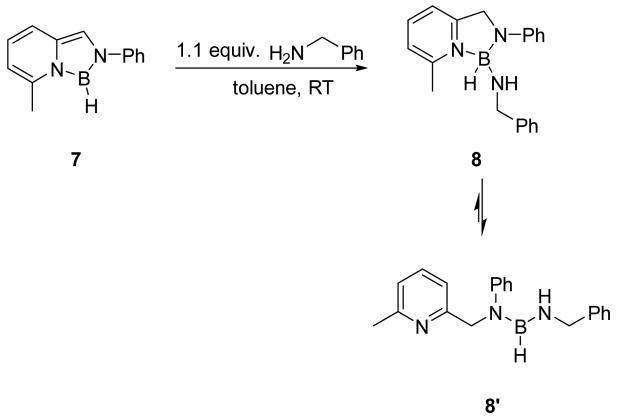

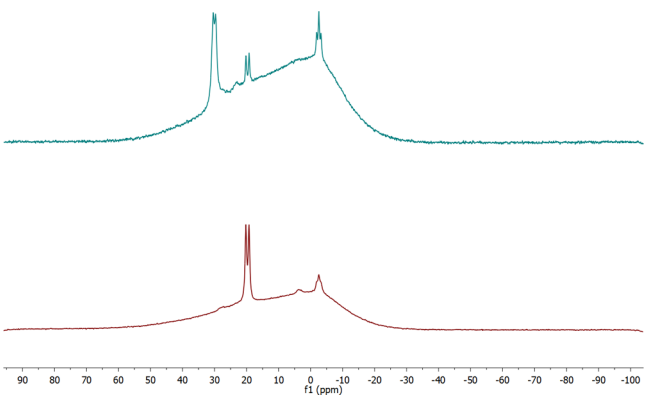

Figure 5. ^{11}B NMR spectra (toluene-d_8) of **7** (red) and 120 min after the addition of 1.1 equiv of benzylamine (green) at 333 K.

Table 5. Comparison of the Calculated ^{11}B NMR Shift and the BH Stretching Vibration of 8′ with the Experimentally Observed Spectroscopic Data

	exp.	DFT
^{11}B NMR (ppm)	30.0	33.4[a]
B–H vibration (cm^{-1})	2491	2516 (2649)[b]
N–H vibration (cm^{-1})	3411	3435 (3617)[b]

[a]Referenced to $Me_3N{\cdot}BH_3$ [b]Calculated vibrations are scaled to account for anharmonicity; unscaled vibrations are given in brackets[16]

DFT calculations indicate that the coordination of benzylamine to the boron center in **7** precedes the NH activation. This coordination is endergonic according to calculations (Figure 6). An adduct of **7** and benzylamine was indeed not observed experimentally.

The coordination of benzylamine to **7** leads to a pyramidalization of the boron center, causing a loss of aromaticity in the five-membered ring. The exergonic NH activation with concomitant rearomatization of the pyridine ring takes place with a low activation barrier of 21 kcal/mol. The activation of **7** by the coordination of benzylamine to it is also reflected in the calculated Kohn–Sham orbitals. The highest occupied Kohn–Sham orbital of **7** is a delocalized π-orbital with two nodal planes. After coordination of benzylamine to **7** the highest occupied Kohn–Sham orbital of the adduct is still a delocalized π-orbital, but its highest coefficient is now found at the C1 position, rendering this position nucleophilic.

Surprisingly, the addition of 1 equiv of benzoic acid to **7** does not lead to protonation of the hydride and H_2 elimination but rather cleanly gives O–H addition product **9** (Scheme 8 and Figure 7). The CH_2 group of the methylene arm appears as an AB signal centered at 4.98 and 4.78 ppm with a $^{3}J_{H-H}$ coupling of 17.9 Hz.

DFT calculations (Figure 8) reveal that the O–H addition requires only a low activation energy of 5.0 kcal/mol. Unlike the case of the amine addition, no stable intermediate in which the carboxylic acid is coordinated to the boron was located. However, the optimized transition state structure reveals that the protonation occurs with concomitant B–O bond formation. The B–O bond length in the transition state is only slightly longer than that in the product **9**.

These structural details show the similarity to the mechanism of the amine addition: Bond activation by **7** is possible but requires prior distortion of the aromaticity of **7**.

DOI: 10.1021/jacs.6b07454
J. Am. Chem. Soc. 2016, 138, 13307–13313

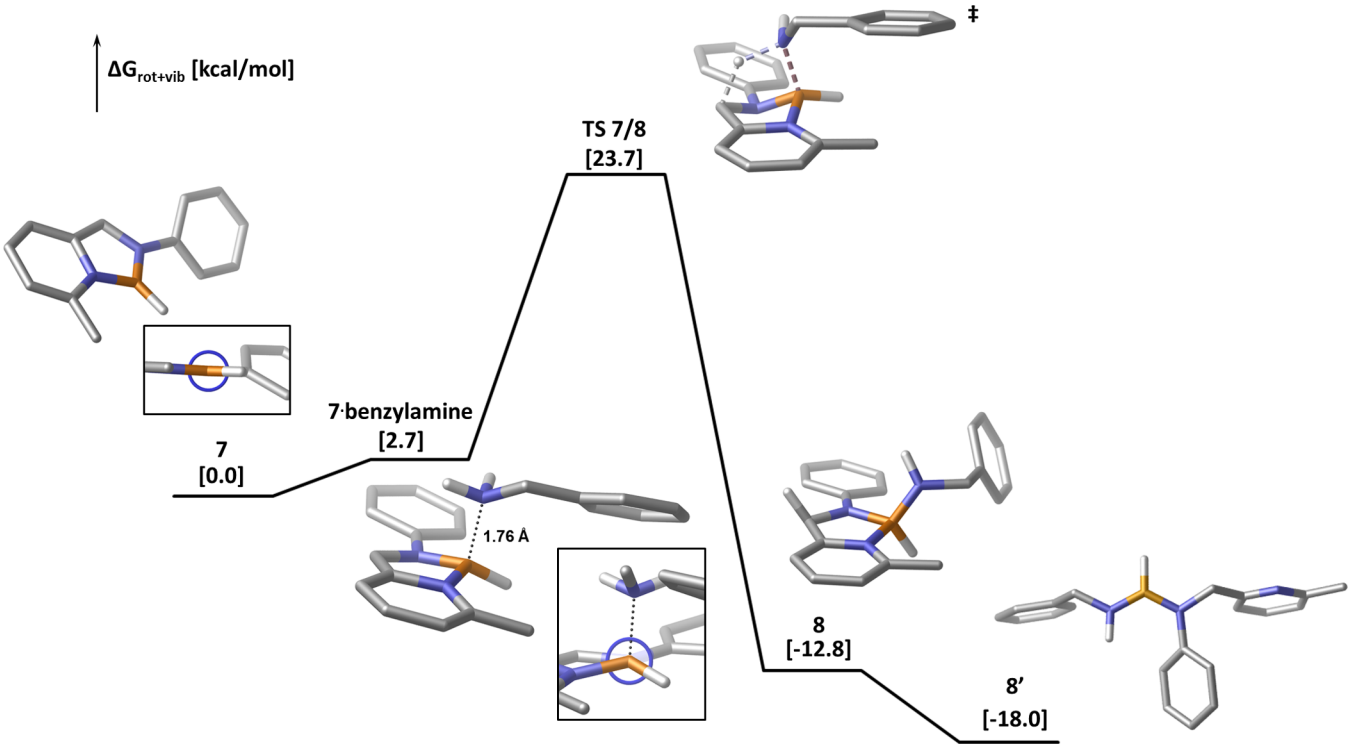

Figure 6. Calculated free energy profile of the reaction of **7** with benzylamine (M06-2X/def2-TZVPP). Newman projections along the B1−N2 bond of **7** and the adduct of **7** with benzylamine visualizing the pyramidalization of the boron center are shown in black frames.

Scheme 8. Reaction of 7 with Benzoic Acid

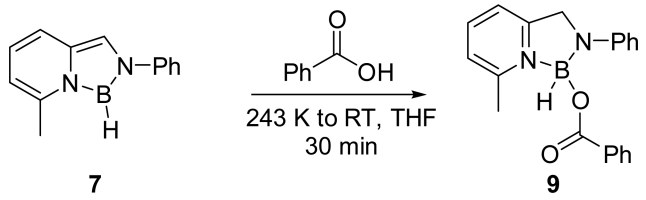

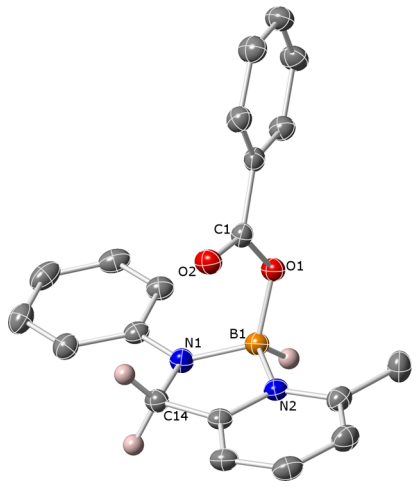

Figure 7. ORTEP of **9** (50% probability ellipsoids, all hydrogens but the ones on C14 and B1 are excluded for clarity). Selected bond lengths (Å) and angles (deg): N1−B1: 1.5048(16), N2−B1: 1.5896(16), B1−O1: 1.5006(15), O1−C1: 1.3289(14), C1−O2: 1.2189(14), N1−C14: 1.4475(14), N2−C15: 1.3462(15), N1−B1−N2: 98.57(9), O1−B1−N1: 114.91(10), O1−B1−N2: 110.96(9).

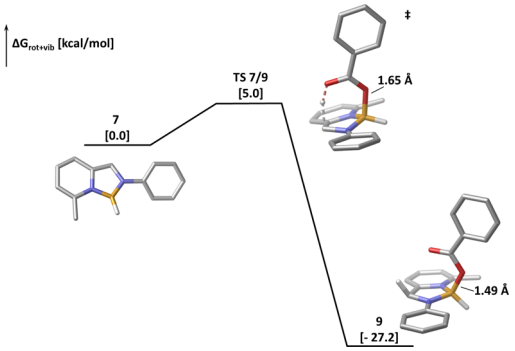

Figure 8. Calculated free energy profile of the reaction of **6** with benzoic acid (M06-2X/def2-TZVPP). The B1−O1 distances in the transition state and in the final product are shown.

In summary, we have documented an unprecedented aromaticity shift of a novel aminoborane and reversal aromaticity shift upon bond activation. NMR experiments and DFT calculations show that the dearomatization of the pyridine ring, involving dihydrogen evolution, leads to a six-π-electron boron-containing heteroaromatic system, compound **7**. Once the aromaticity of the boracycle **7** is disturbed by coordination of an electron donor to the boron center, the C1 position becomes nucleophilic, and N−H σ-bond activation (or O−H addition) becomes possible, leading to rearomatization of the pyridine ring with concomitant dearomatization of the boracycle. The whole reaction sequence can be described as unprecedented bond activation via aromaticity shift. Moreover, this process involves boron, rather than a metal center. We believe that the results reported herein raise the possibility of the design of a novel class of organocatalysts operating via reversible aromaticity shifts.

DOI: 10.1021/jacs.6b07454
J. Am. Chem. Soc. 2016, 138, 13307−13313

EXPERIMENTAL DETAILS

General Specifications. All manipulations were carried out under a nitrogen atmosphere using standard Schlenk and glovebox techniques if not indicated otherwise. All chemicals for which synthesis is not given were commercially available from Aldrich, Acros, or STREM and were used as received without further purification. Tetrahydrofuran, toluene, benzene, dioxane, and *n*-pentane were refluxed over sodium/benzophenone, distilled under argon atmosphere, and stored over 4 Å molecular sieves. Methylene chloride was purchased from J. T. Baker as HPLC ultra gradient and dried over 4 Å molecular sieves. Deuterated solvents were degassed with argon and kept in the glovebox over 4 Å molecular sieves. NMR spectra were recorded on Bruker AMX-300, AMX-400, and AMX-500 NMR spectrometers. ^{1}H and ^{13}C NMR chemical shifts are referenced to TMS or to residual solvent resonance peaks. ^{11}B NMR chemical shifts are referenced to $Et_2O{\cdot}BF_3$ as external standard. In the ^{13}C DEPTQ NMR experiments, signals of primary and tertiary carbons are phased down, and signals of secondary and quaternary carbons are phased up. IR spectra were recorded on a Nicolet FT-IR spectrophotometer.

Synthesis of ***4****.* 6-Methylpyridine-2-carboxaldehyde (2.4 g, 20.0 mmol) was dissolved in CH_2Cl_2 (20 mL), and molecular sieves (4 Å) were added. Aniline (1.8 mL, 1.8 g, 20.0 mmol, 1 equiv) was added, and the reaction mixture was stirred for 16 h at RT. The mixture was filtered and the solvent removed under reduced pressure. The residue was dissolved in MeOH (20 mL), and $NaBH_4$ (0.76 g, 20 mmol, 1 equiv) was added. The mixture was stirred at RT for 15 min. The reaction was quenched by addition of acetic acid (2 mL) at 0 °C, and all volatiles were removed under reduced pressure. The remaining solid was suspended in ethyl acetate (20 mL), and a K_2CO_3 solution (10 wt %, 20 mL) was added. The organic phase was separated and the aqueous phase washed three times with ethyl acetate (20 mL). The organic phases were combined, dried over $MgSO_4$, and the solvent was removed under reduced pressure. The crude product was purified by recrystallization from ethyl acetate/hexane yielding **4** (3.5 g, 17.7 mmol, 88%) as a colorless solid. ^{1}H NMR (500 MHz, $CDCl_3$) 2.62 (s, 3H, Py−CH_3), 4.46 (br s, 2H, NHPh−CH_2Py), 4.80 (br s, 1H, N(H)Ph−CH_2Py), 6.71 (d, J = 8.5 Hz, 2H, ArH), 6.79−6.73 (m, 1H, ArH), 7.07 (d, J = 7.6 Hz, 1H, Py−H), 7.17 (d, J = 7.7 Hz, 1H, Py−H), 7.22 (t, J = 7.6 Hz, 2H, ArH), 7.55 (t, J = 7.7 Hz, 1H, Py−H). ^{13}C {^{1}H} NMR (126 MHz, $CDCl_3$) δ 24.5 (s, Py−CH_3), 49.4 (s, NHPh−CH_2Py), 113.1, 117.5, 118.5, 121.6, 129.25, 136.9, 148.0, 157.8, 158.0.

Synthesis of ***6****.* $Me_2S{\cdot}BH_3$ (0.47 mL, 0.38 g, 5.0 mmol) was dissolved in benzene (10 mL), and the mixture was cooled in an ice−water bath. Br_2 (0.13 mL, 0.40 g, 2.5 mmol) dissolved in benzene (10 mL) was added dropwise over 30 min. The reaction mixture was warmed to RT and stirred at this temperature for 2 h. **4** (0.98 g, 5 mmol) was dissolved and added to the mixture. The reaction mixture was stirred for 16 h and filtered under nitrogen. The residue was washed with benzene (3 × 5 mL) and dried. Some of the crude product (0.29 g, 1 mmol) was suspended in benzene (2 mL), and NEt_3 (0.13 mL, 0.1 g, 1 mmol) was added and the mixture stirred for 15 min. The reaction mixture was extracted with benzene (5 × 2 mL) and dried. Crystallization from CH_2Cl_2/pentane yielded **6** (0.13 g, 0.06 mmol, 60%) as a yellow crystalline powder. Single crystals suitable for X-ray analysis were obtained by keeping a concentrated solution of **6** in toluene overlaid with pentane at −38 °C. ^{1}H NMR (500 MHz, $CDCl_3$) 2.77 (s, 3H, Py−CH_3), 3.56 (bm, 1H, BH), 3.75 (bm, 1H, BH), 4.79 (s, 2H, N(BH_2)Ph−CH_2Py), 6.59 (t, J = 7.2 Hz, 1H, Ar−H), 6.64 (d, J = 7.9 Hz, 2H, ArH), 7.23 (dd, J = 7.9, 7.2 Hz, 2H, ArH), 7.30 (d, J = 7.8 Hz, 1H, Py−H), 7.40 (d, J = 7.8 Hz, 1H, Py−H), 7.86 (t, J = 7.8 Hz, 1H, Py−H). ^{11}B NMR (160 MHz, $CDCl_3$) −4.10 (t, $^{1}J_{B-H}$ = 103.2 Hz). ^{13}C NMR (126 MHz, $CDCl_3$) 20.9 (s, Py−CH_3), 53.3 (s, N(BH_2)Ph−CH_2Py), 76.96, 77.22, 77.47, 112.56, 114.09, 118.55, 124.31, 129.19, 140.14, 149.16, 154.01, 157.61. ^{1}H NMR (500 MHz, C_6D_6) 2.25 (s, 3H, Py−CH_3) 3.90−4.70 (s, 2H, N(BH_2)Ph−CH_2Py overlapping with bm, 2H, BH_2), 6.05 (d, J = 7.8 Hz, 1H, Py−H), 6.10 (d, J = 7.8 Hz, 1H, Py−H), 6.57 (t, J = 7.8 Hz, 1H, Py−H), 6.89 (t, J = 7.2 Hz, 1H, Ar−H), 7.05 (d, J = 7.9 Hz, 2H, ArH), 7.51 (dd, J = 7.9, 7.2 Hz, 2H, ArH). ^{11}B NMR (160 MHz, $CDCl_3$) −2.6 (t, $^{1}J_{B-H}$ = 101.6 Hz). IR (KBr pellet, cm^{-1}) 2290 (br, ν_{B-H}). HR-ESI-MS: m/z = 211.1416 (calcd for $[C_{13}H_{16}BN_2]^+$ = 211.141).

X-ray Structure Determination of ***6****.* Crystal data: $C_{13}H_{15}BN_2$, yellow chunk, 0.462 × 0.258 × 0.140 mm^3, monoclinic $C2/c$, a = 22.7448(19) Å, b = 6.4330(5) Å, c = 16.2309(13) Å, β = 105.714(5)°, from 9668 reflections, T = 100(2) K, V = 2286.1(3) Å^3, Z = 8, F_w = 210.08, D_c = 1.221 Mg·m^{-3}, μ = 0.072 mm^{-1}. Data collection and processing: Bruker KappaApexII diffractometer, Mo Kα (λ = 0.71073 Å), $-24 \le h \le 28$, $-7 \le k \le 8$, $-20 \le l \le 20$, frame scan width = 0.5°, scan speed 1.0° per 240 s, 9668 reflections collected, 2650 independent reflections (R_{int} = 0.0620). The data were processed with SAINT. Solution and refinement: Structure solved with SHELXS. Full matrix least-squares refinement based on F^2 with SHELXL on 146 parameters with no restraints gave final R_1 = 0.0510 (based on F^2) for data with $I > 2\sigma(I)$ and wR_2 = 0.1213 on 2412 reflections, goodness-of-fit on F^2 = 1.010 largest electron density peak 0.258 e Å^{-3}. Largest hole −0.199 e Å^{-3}.

Formation of ***7****.* Method A: Complex **6** (21.0 mg, 0.1 mmol) was dissolved in C_6D_6 (0.5 mL) and transferred to a NMR Young tube. The suspension was heated to 333 K for 16 h and analyzed by ^{1}H and ^{11}B NMR. Method B: Complex **5** (290.0 mg, 1 mmol) was suspended in benzene (0.5 mL) and vigorously stirred for 48 h at RT. NEt_3 (0.13 mL, 0.1 g, 1 mmol) was added and the mixture stirred for 15 min. The solvent was removed under reduced pressure and the solid extracted with *n*-pentane (3 × 5 mL). The extract was completely dried, and **7** (47.0 mg, 0.23 mmol, 23%) obtained as orange solid. ^{1}H NMR (500 MHz, C_6D_6) 2.00 (s, 3H, Py−CH_3), 5.51 (d, J = 6.2 Hz, 1H, *meta* Py−H), 6.19 (dd, J = 9.3, 6.2 Hz, 1H, *para* Py−H), 6.68 (s, 1H, N(BH)Ph−CHPy), 6.70 (d, J = 9.3 Hz, 1H, *meta* Py−H), 6.97 (t, J = 7.3 Hz, 1H, ArH), 7.15 (t, J = 7.8 Hz, 2H, ArH), 7.33 (d, J = 7.7 Hz, 2H, ArH). ^{11}B NMR (160 MHz, C_6D_6) 19.7 (d, $^{1}J_{B-H}$ = 155.1 Hz). ^{13}C NMR (126 MHz, C_6D_6) 12.2 (s, Py−CH_3), 97.0, 98.3, 107.6, 108.3, 112.2, 113.1, 116.4, 121.2, 121.5. IR (KBr pellet, cm^{-1}) 2607 (br, ν_{B-H}). HR-ESI-MS: m/z = 209.1260 (calcd for $[C_{13}H_{14}BN_2]^+$ = 209.125). A more detailed description of the *in situ* NMR studies is provided in the Supporting Information.

Formation of ***8****.* Complex **7** (15.0 mg, 0.072 mmol) was dissolved in toluene-d_8 (0.6 mL) and transferred to a NMR Young tube. Benzylamine (8.6 μL, 8.5 mg, 0.080 mmol, 1.1 equiv) was added and the tube placed in the precooled NMR spectrometer. The reaction progress at 273 K was followed by ^{1}H NMR spectroscopy. ^{1}H NMR (500 MHz, toluene-d_8) 2.48 (s, 3H, Py−CH_3), 3.47 (bt, 1H, NHCH_2Ph), 4.11 (d, J = 7.3 Hz, 2H, NHCH2Ph), 4.76 (s, 2H, N(BHNHCH_2Ph)Ph−CH2Py), 6.61 (d, J = 7.5 Hz, 1H), 6.80 (d, J = 9.2 Hz, 1H), 6.99−6.93 (m, 3H), 7.13−7.04 (m, 5H), 7.40 (d, J = 7.8 Hz, 2H), 7.54 (t, J = 7.7 Hz, 1H). ^{11}B NMR (160 MHz, toluene-d_8) 30.0 (d, $^{1}J_{B-H}$ = 114.2 Hz). IR (KBr pellet, cm^{-1}) 2491 (br, ν_{B-H}), 3411 (br, ν_{N-H}). A more detailed description of the *in situ* NMR studies is provided in the Supporting Information.

Synthesis of ***9****.* Complex **7** (48.0 mg, 023 mmol) was dissolved in THF (4 mL) and cooled to 243 K. A solution of benzoic acid (28.2 mg, 0.23 mmol, 1 equiv) in THF (2 mL) precooled to 243 K was added dropwise. The reaction mixture was allowed to warm to RT, stirred for 30 min, and filtered through Celite. The solvent was removed under vacuum and the residue redissolved in methylene chloride (1 mL) and overlaid with *n*-pentane (5 mL). Upon storing at 243 K, orange crystals were formed. Upon decantation of the solution and drying of the residue under vacuum **9** was obtained (60.0 mg, 83%) as an orange solid. Crystals suitable for X-ray analysis were obtained by layering a $CDCl_3$ solution of **9** with diethyl ether. ^{1}H NMR (500 MHz, $CDCl_3$) 2.86 (s, 3H, Py−CH_3), AB system centered at 4.78 (d, J = 17.8 Hz) and 4.98 78 (d, J = 17.8 Hz), 6.66 (t, J = 7.2 Hz, 1H), 6.95 (d, J = 7.9 Hz, 2H), 7.24 (dd, J = 8.5, 7.3 Hz, 2H), 7.35 (m, 3H), 7.46 (dd, J = 10.5, 4.3 Hz, 1H), 7.54 (d, J = 7.9 Hz, 1H), 7.97 (t, J = 7.8 Hz, 1H), 8.00−8.04 (m, 1H). ^{11}B NMR (160 MHz, $CDCl_3$) δ 2.94 (d, $^{1}J_{B-H}$ = 118.5 Hz). ^{13}C NMR (126 MHz, $CDCl_3$) 20.65 (s, Py−CH_3), 52.62, 76.79, 77.04, 77.29, 112.92, 115.51, 124.60, 127.94, 128.16, 129.03, 129.67, 129.89, 131.78, 133.35, 141.34, 147.70, 153.60, 159.48, 168.27. IR (KBr pellet, cm^{-1}) 1695 ($\nu_{C=O}$), 2365 (br, ν_{B-H}, overlapping with ν_{CO_2}).

X-ray Structure Determination of ***9****.* Crystal data: $C_{20}H_{19}BN_2O_2$ colorless plate, 0.08 × 0.08 × 0.04 mm^3, monoclinic $P2(1)/c$, a = 11.7679(1) Å, b = 11.3623(1) Å, c = 13.0103(1) Å, β = 104.0256(8)°,

DOI: 10.1021/jacs.6b07454
J. Am. Chem. Soc. 2016, 138, 13307−13313

from 11 473 reflections, T = 100(2) K, V = 1687.75(2) Å^3, Z = 4, F_w = 330.18, D_c = 1.299 Mg m^{-3}, μ = 0.665 mm^{-1}. Data collection and processing: Rigaku XtaLab Pro diffractometer, Cu Kα (λ = 1.54184 Å), $-14 \le h \le 15$, $-14 \le k \le 14$, $-16 \le l \le 16$, frame scan width = 0.5°, scan speed 10.0° per 14.14 s (High θ) or 3.54 s (Low θ), typical peak mosaicity 0.7°, 23 738 reflections collected, 3672 independent reflections (R_{int} = 0.0343). The data were processed with CrysAlis^{Pro}. Solution and refinement: Structure solved with SHELXT-2013. Full matrix least-squares refinement based on F^2 with SHELXL on 240 parameters with 0 restraints gave final R_1 = 0.0392 (based on F^2) for data with $I > 2\sigma(I)$ and wR_2 = 0.0993 on 3672 reflections, goodness-of-fit on F^2 = 1.077, largest electron density peak 0.194 e Å^{-3}, largest hole −0.217 e Å^{-3}.

Computational Details. All computations were performed with the meta hybrid functional M06-2X together with a def2-TZVPP basis set.[27,28] Thermodynamic properties were obtained at the same level of theory from a frequency calculation. This level of theory was also used for the population analysis and NMR calculations, the latter using the GIAO method.[29] Previous studies revealed that taking infinitely separated reactants as reference states leads to an overestimation of the entropy loss in bimolecular reactions, mainly because the loss of translational degrees of freedom is overestimated.[30] We therefore decided to take only the vibrational and rotational degrees of freedom into account when estimating the free energy changes. This is denoted in the manuscript as $\Delta G_{vib+rot}$. All free energies are calculated under standard conditions unless otherwise noted. Minima and transition states were characterized by the absence and presence of one imaginary frequency, respectively. The "ultrafine" (i.e., a pruned (99 590)) grid was used for all calculations. All calculations were performed using Gaussian 09, revision D.01.[31]

■ ASSOCIATED CONTENT

Supporting Information

The Supporting Information is available free of charge on the ACS Publications website at DOI: 10.1021/jacs.6b07454.

Experimental details, X-ray data, and computational details including the Cartesian coordinates and the electronic energies of the calculated structures (PDF)

Crystallographic information file for compounds **6** and **9** (CIF)

■ AUTHOR INFORMATION

Corresponding Author

*david.milstein@weizmann.ac.il

Notes

The authors declare no competing financial interest.

■ ACKNOWLEDGMENTS

This research was supported by the Israel Science Foundation and by the Kimmel Center for Molecular Design. U.G. thanks the DAAD for a Post Doctoral Fellowship and the Feinberg Graduate School for a Senior Post-Doctoral Award. D.M. holds the Israel Matz Professorial Chair of Organic Chemistry.

■ REFERENCES

(1) Review: Khusnutdinova, J. R.; Milstein, D. *Angew. Chem., Int. Ed.* **2015**, *54*, 12236.

(2) Milstein, D. *Philos. Trans. R. Soc. A* **2015**, *373*, 20140189.

(3) Maire, P.; Büttner, T.; Breher, F.; LeFloch, P.; Grützmacher, H. *Angew. Chem., Int. Ed.* **2005**, *44*, 6318; *Angew. Chem.* **2005**, *117*, 6477.

(4) Kimura, T.; Koiso, N.; Ishiwata, K.; Kuwata, S.; Ikariya, T. *J. Am. Chem. Soc.* **2011**, *133*, 8880.

(5) (a) Musa, S.; Shaposhnikov, I.; Cohen, S.; Gelman, D. *Angew. Chem., Int. Ed.* **2011**, *50*, 3533. (b) Silantyev, G. A.; Filippov, O. A.; Musa, S.; Gelman, D.; Belkova, N. V.; Weisz, K.; Epstein, L. M.; Shubina, E. S. *Organometallics* **2014**, *33*, 5964.

(6) (a) Zhang, J.; Leitus, G.; Ben-David, Y.; Milstein, D. *J. Am. Chem. Soc.* **2005**, *127*, 10840. (b) Gunanathan, C.; Milstein, D. *Acc. Chem. Res.* **2011**, *44*, 588.

(7) (a) Kohl, S. W.; Weiner, L.; Schwartsburd, L.; Konstantinovski, L.; Shimon, L. J. W.; Ben-David, Y.; Iron, M. A.; Milstein, D. *Science* **2009**, *324*, 74. (b) Li, J.; Shiota, Y.; Yoshizawa, K. *J. Am. Chem. Soc.* **2009**, *131*, 13584. (c) Sandhya, K. S.; Suresh, C. H. *Organometallics* **2011**, *30*, 3888.

(8) Gunanathan, C.; Ben-David, Y.; Milstein, D. *Science* **2007**, *317*, 790.

(9) Cho, D.; Ko, K. C.; Lee, J. Y. *Organometallics* **2013**, *32*, 4571.

(10) (a) Ben-Ari, E.; Leitus, G.; Shimon, L. J. W.; Milstein, D. *J. Am. Chem. Soc.* **2006**, *128*, 15390. (b) Schwartsburd, L.; Iron, M. A.; Konstantinovski, L.; Diskin-Posner, Y.; Leitus, G.; Shimon, L. J. W.; Milstein, D. *Organometallics* **2010**, *29*, 3817. (c) Schwartsburd, L.; Iron, M. A.; Konstantinovski, L.; Ben-Ari, E.; Milstein, D. *Organometallics* **2011**, *30*, 2721.

(11) Khaskin, E.; Iron, M. A.; Shimon, L. J. W.; Zhang, J.; Milstein, D. *J. Am. Chem. Soc.* **2010**, *132*, 8542.

(12) Anaby, A.; Butschke, B.; Ben-David, Y.; Shimon, L. J. W.; Leitus, G.; Feller, M.; Milstein, D. *Organometallics* **2014**, *33*, 3716.

(13) Gunanathan, C.; Milstein, D. *Chem. Rev.* **2014**, *114*, 12024.

(14) (a) Lu, G.; Li, H.; Zhao, L.; Huang, F.; Schleyer, P. v. R.; Wang, Z.-X. *Chem. - Eur. J.* **2011**, *17*, 2038. (b) Li, H.; Wen, M.; Lu, G.; Wang, Z.-X. *Dalton Trans.* **2012**, *41*, 9091.

(15) For a recent example of a phosphorous-containg PN borane complex, see Devillard, M.; Alvarez Lamsfus, C.; Vreeken, V.; Maron, L.; van der Vlugt, J. I. *Dalton Trans.* **2016**, *45*, 10989.

(16) (a) Chang, M.-C.; Otten, E. *Organometallics* **2016**, *35*, 534−542. (b) Bonnier, C.; Piers, W. E.; Parvez, M. *Organometallics* **2011**, *30*, 1067.

(17) Kesharwani, M. K.; Brauer, B.; Martin, J. M. L. *J. Phys. Chem. A* **2015**, *119*, 1701.

(18) For details, see the Supporting Information

(19) Grimme, S.; Kruse, H.; Goerigk, L.; Erker, G. *Angew. Chem.* **2010**, *122*, 1444.

(20) Schleyer, P. v. R.; Maerker, C.; Dransfeld, A.; Jiao, H.; Hommes, N. J. R. v. E. *J. Am. Chem. Soc.* **1996**, *118*, 6317.

(21) Hertz, V. M.; Bolte, M.; Lerner, H. W.; Wagner, M. *Angew. Chem., Int. Ed.* **2015**, *54*, 8800.

(22) Review: Messersmith, R. E.; Tovar, J. D. *J. Phys. Org. Chem.* **2015**, *28*, 378.

(23) Braunschweig, H.; Damme, A.; Jimenez-Halla, J. O. C.; Pfaffinger, B.; Radacki, K.; Wolf, J. *Angew. Chem., Int. Ed.* **2012**, *51*, 10034−10037.

(24) Schleyer, P. v. R.; Pühlhofer, F. *Org. Lett.* **2002**, *4*, 2873−2876.

(25) An analysis of the frontier Kohn−Sham orbitals of **2** and **7** can be found in the Supporting Information.

(26) According to a calibration using $Et_2O{\cdot}BF3$ as external standard, the chemical shifts of **6** and **7** in toluene-d_8 are the same as those in benzene-d_6.

(27) Zhao, Y.; Truhlar, D. G. *Theor. Chem. Acc.* **2008**, *120*, 215.

(28) Weigend, F.; Ahlrichs, R. *Phys. Chem. Chem. Phys.* **2005**, *7*, 3297.

(29) Ditchfield, R. *Mol. Phys.* **1974**, *27*, 789.

(30) Mondal, B.; Neese, F.; Ye, S. *Inorg. Chem.* **2015**, *54*, 7192. and the literature cited therein.

(31) Frisch, M. J.; Trucks, G. W.; Schlegel, H. B.; Scuseria, G. E.; Robb, M. A.; Cheeseman, J. R.; Scalmani, G.; Barone, V.; Mennucci, B.; Petersson, G. A.; Nakatsuji, H.; Caricato, M.; Li, X.; Hratchian, H. P.; Izmaylov, A. F.; Bloino, J.; Zheng, G.; Sonnenberg, J. L.; Hada, M.; Ehara, M.; Toyota, K.; Fukuda, R.; Hasegawa, J.; Ishida, M.; Nakajima, T.; Honda, Y.; Kitao, O.; Nakai, H.; Vreven, T.; Montgomery, J. A., Jr.; Peralta, J. E.; Ogliaro, F.; Bearpark, M.; Heyd, J. J.; Brothers, E.; Kudin, K. N.; Staroverov, V. N.; Kobayashi, R.; Normand, J.; Raghavachari, K.; Rendell, A.; Burant, J. C.; Iyengar, S. S.; Tomasi, J.; Cossi, M.; Rega, N.; Millam, J. M.; Klene, M.; Knox, J. E.; Cross, J. B.; Bakken, V.; Adamo, C.; Jaramillo, J.; Gomperts, R.; Stratmann, R. E.; Yazyev, O.; Austin, A. J.; Cammi, R.; Pomelli, C.; Ochterski, J. W.; Martin, R. L.; Morokuma, K.; Zakrzewski, V. G.; Voth, G. A.; Salvador, P.; Dannenberg, J. J.; Dapprich, S.; Daniels, A. D.; Farkas, O.; Foresman, J. B.; Ortiz, J. V.; Cioslowski, J.; Fox, D. J. *Gaussian 09*, revision D.01; Gaussian, Inc.: Wallingford, CT, 2009.

DOI: 10.1021/jacs.6b07454
J. Am. Chem. Soc. 2016, 138, 13307−13313